



This is a repository copy of *Temperature characterisation of spectroscopic InGaP X-ray photodiodes*.

White Rose Research Online URL for this paper:  
<http://eprints.whiterose.ac.uk/167001/>

Version: Accepted Version

---

**Article:**

Butera, S., Lioliou, G., Krysa, A.B. [orcid.org/0000-0001-8320-7354](https://orcid.org/0000-0001-8320-7354) et al. (1 more author) (2018) Temperature characterisation of spectroscopic InGaP X-ray photodiodes. Nuclear Instruments and Methods in Physics Research Section A: Accelerators, Spectrometers, Detectors and Associated Equipment, 908. pp. 277-284. ISSN 0168-9002

<https://doi.org/10.1016/j.nima.2018.08.064>

---

Article available under the terms of the CC-BY-NC-ND licence (<https://creativecommons.org/licenses/by-nc-nd/4.0/>).

**Reuse**

This article is distributed under the terms of the Creative Commons Attribution-NonCommercial-NoDerivs (CC BY-NC-ND) licence. This licence only allows you to download this work and share it with others as long as you credit the authors, but you can't change the article in any way or use it commercially. More information and the full terms of the licence here: <https://creativecommons.org/licenses/>

**Takedown**

If you consider content in White Rose Research Online to be in breach of UK law, please notify us by emailing [eprints@whiterose.ac.uk](mailto:eprints@whiterose.ac.uk) including the URL of the record and the reason for the withdrawal request.



[eprints@whiterose.ac.uk](mailto:eprints@whiterose.ac.uk)  
<https://eprints.whiterose.ac.uk/>

1 **Temperature characterisation of spectroscopic InGaP X-ray**  
2 **photodiodes**

3  
4 S. Butera<sup>1,\*</sup>, G. Lioliou<sup>1</sup>, A. B. Krysa<sup>2</sup>, A. M. Barnett<sup>1</sup>

5  
6 <sup>1</sup>Space Research Group, School of Engineering and Informatics, University of Sussex,  
7 Brighton, BN1 9QT, UK.

8 <sup>2</sup>EPSRC National Epitaxy Facility, University of Sheffield, Mappin Street, Sheffield,  
9 S1 3JD, UK.

10  
11 Email: S.Butera@sussex.ac.uk (S. Butera)

12 Tel.: +441273872568

13  
14 **Abstract.** In this paper for the first time, an InGaP photodiode was used in a high  
15 temperature tolerant X-ray spectrometer. The use of InGaP in X-ray spectrometers  
16 shows a significant advance within this field allowing operation up to 100 °C. Such  
17 results are particularly important since GaP and InP (the InGaP binary parent  
18 compounds) are not spectroscopic even at room temperature. The best energy  
19 resolution (smallest FWHM) at 5.9 keV for the InGaP spectrometer was 1.27 keV at  
20 100 °C and 770 eV at 20 °C, when the detector was reverse biased at 5 V. The observed  
21 FWHM were higher than the expected statistically limited energy resolutions indicating  
22 that other sources of noise contributed to the FWHM broadening. The spectrometer's  
23 Si preamplifier electronics was the limiting factor for the FWHM rather than the InGaP  
24 photodiode itself. The InGaP electron-hole pair creation energy ( $\epsilon_{InGaP}$ ) was  
25 experimentally measured across the temperature range 100 °C to 20 °C.  $\epsilon_{InGaP}$  was 4.94  
26 eV  $\pm$  0.06 eV at 20 °C.

27  
28 **Keywords:** InGaP; X-ray spectroscopy; electron-hole pair creation energy;  
29 semiconductor.

30  
31  
32 **1. INTRODUCTION**

33

---

\* Author to whom correspondence should be addressed.

34 High-resolution X-ray astronomy and X-ray fluorescence spectroscopy [1] have been  
35 made possible because of the use of photon counting X-ray spectrometers. The ability  
36 to determine the energy of individual X-ray photons and the number of the detected X-  
37 ray photons at a particular energy can be essential in space missions. These attributes  
38 are particularly useful to study planetary surfaces, magnetospheres, and solar physics,  
39 as well as for terrestrial applications such as industrial monitoring and non-destructive  
40 testing. The use of wide bandgap materials in such spectrometers is attractive because  
41 such materials can have low thermally generated leakage currents; as such they can  
42 operate at high temperatures without cooling systems thus resulting in more compact,  
43 lower mass, and lower power instrumentation.

44  
45 High energy resolution and temperature tolerant photon counting X-ray spectrometers  
46 have been reported using various wide bandgap semiconductor detectors coupled to  
47 low-noise preamplifier electronics [2, 3, 4, 5]. Lioliou et al. [2] reported a GaAs diode  
48 with energy resolution (Full Width at Half Maximum, FWHM) at 5.9 keV of 840 eV at  
49 60 °C. Barnett et al. [3] demonstrated an  $\text{Al}_{0.8}\text{Ga}_{0.2}\text{As}$  detector with energy resolution  
50 at 5.9 keV of 2.2 keV at 90 °C. In both cases the Si preamplifier electronics were also  
51 operated uncooled at the same temperature as the compound semiconductor  
52 photodetector. A SiC X-ray spectrometer with an energy resolution at 5.9 keV of  
53 233 eV at 100 °C has also been developed by Bertuccio et al. [4]. Recently, another  
54 wide bandgap semiconductor,  $\text{Al}_{0.52}\text{In}_{0.48}\text{P}$ , has shown exceptional promise as a newly  
55 emerging material for photon counting X-ray spectroscopy. Butera et al. [5] reported  
56 an  $\text{Al}_{0.52}\text{In}_{0.48}\text{P}$  detector spectrometer with an energy resolution at 5.9 keV of 1.57 keV  
57 at 100 °C and 0.90 keV at 20 °C. The spectroscopic performance of CdTe and CdZnTe  
58 detectors has also been investigated at high temperature. Squillante et al. [6] reported  
59 a CdTe spectrometer with an energy resolution at 122 keV of 53 keV at 92 °C.  
60 Egarievwe et al. [7] developed a CdZnTe spectrometer with an energy resolution at 32  
61 keV of 9.4 keV at 70 °C. CdTe and CdZnTe detectors have been widely developed for  
62 room temperature X-ray spectroscopy. For example, Zappettini et al. [8] demonstrated  
63 CdZnTe detectors with an energy resolution at 59.5 keV of 2.5 keV using low-noise  
64 application specific integrated circuit (ASIC) readout electronics. Abbene et al. [9]  
65 reported a CdZnTe structure showing energy resolutions of 3.8% (2.26 keV) and 3.2%  
66 (3.91 keV) at 59.5 keV and 122.1 keV, respectively, at low count rate. Recently an  
67  $\text{In}_{0.5}\text{Ga}_{0.5}\text{P}$  X-ray photodiode was also demonstrated to be spectroscopic at room

68 temperature when coupled to a low noise charge sensitive preamplifier [10]. This was  
69 particularly surprising given that its parent materials InP and GaP had been previously  
70 found to be non-spectroscopic [11, 12, 13, 14]. The use of  $\text{In}_{0.5}\text{Ga}_{0.5}\text{P}$  is important  
71 because it has large X-ray and  $\gamma$ -ray attenuation coefficients leading to high quantum  
72 detection efficiencies per unit thickness [15, 16].

73

74 In this paper, for the first time, an  $\text{In}_{0.5}\text{Ga}_{0.5}\text{P}$   $\text{p}^+\text{-i-n}^+$  mesa photodiode was coupled to  
75 a custom-made low-noise charge-sensitive preamplifier and investigated for its  
76 performance at high temperature (from 100 °C to 20 °C). The material's electron-hole  
77 pair creation energy was also determined. The performance of the spectrometer was  
78 analysed under the illumination of a 192 MBq  $^{55}\text{Fe}$  radioisotope X-ray source over the  
79 temperature range using different shaping times and applied biases. At 100 °C, the best  
80 energy resolution at 5.9 keV was 1.27 keV, which improved to 770 eV at 20 °C. The  
81 different noise contributors to these determined energy resolutions were computed and  
82 are discussed in detail. The electron-hole pair creation energy,  $\varepsilon_{\text{InGaP}}$ , was measured  
83 using a dedicated experiment. It was found that  $\varepsilon_{\text{InGaP}} = 4.94 \text{ eV} \pm 0.06 \text{ eV}$  at 20 °C.  
84  $\varepsilon_{\text{InGaP}}$  is the average energy consumed in the generation of an electron-hole pair during  
85 the creation of a charge cloud of electron-hole pairs upon absorption of an X-ray photon  
86 within  $\text{In}_{0.5}\text{Ga}_{0.5}\text{P}$ .

87

## 88 **2. EXPERIMENTAL**

### 89 **2.1 STRUCTURE DESIGN**

90

91 An  $\text{In}_{0.5}\text{Ga}_{0.5}\text{P}$   $\text{p}^+\text{-i-n}^+$  epilayer was grown on a heavily doped  $\text{n}^+$  GaAs substrate by  
92 low-pressure (150 Torr) metalorganic vapour phase epitaxy using trimethylgallium,  
93 trimethylindium, arsine, and phosphine as precursors, and hydrogen as a carrier gas.  
94 Disilane and dimethylzinc:triethylamine were used for n- and p-doping, respectively.  
95 The epitaxial surface of the substrate had an orientation of (100) with a miscut angle of  
96  $10^\circ$  towards the GaAs  $\langle 111 \rangle$  plane terminating with Ga atoms. The unintentionally  
97 doped i layer (thickness of 5  $\mu\text{m}$ ) was between a top  $\text{p}^+$  layer (thickness of 0.2  $\mu\text{m}$ ;  
98 doping concentration of  $2 \times 10^{18} \text{ cm}^{-3}$ ) and a bottom  $\text{n}^+$  layer (thickness of 0.1  $\mu\text{m}$ ;  
99 doping concentration of  $2 \times 10^{18} \text{ cm}^{-3}$ ). It has to be noted that the thickness of the  $\text{p}^+$   
100 and  $\text{n}^+$  layers were as thin as possible such to decrease the absorption in these layers.  
101 The thicknesses for the  $\text{p}^+$  layer (0.2  $\mu\text{m}$ ) and  $\text{n}^+$  layer (0.1  $\mu\text{m}$ ) were chosen based on

102 our own experience of growth of high quality  $\text{In}_{0.5}\text{Ga}_{0.5}\text{P}$ . The thickness of the i layer,  
 103 instead, was thick to increase the absorption, and consequently the quantum efficiency,  
 104 in this layer. It has to be highlighted that the  $\text{In}_{0.5}\text{Ga}_{0.5}\text{P}$  device is the thickest i layer  
 105  $\text{In}_{0.5}\text{Ga}_{0.5}\text{P}$  photodiode so far reported; i layers thicker than  $5\ \mu\text{m}$  may be produced in  
 106 the future. On top of the  $\text{In}_{0.5}\text{Ga}_{0.5}\text{P}$   $\text{p}^+\text{-i-n}^+$  epilayer, a thin  $\text{p}^+$  GaAs layer (thickness  
 107 of  $0.01\ \mu\text{m}$ ; doping concentration of  $1 \times 10^{19}\ \text{cm}^{-3}$ ) was grown to help achieve a good  
 108 top Ohmic contact. n type GaAs, n type  $\text{In}_{0.5}\text{Ga}_{0.5}\text{P}$  and unintentionally doped  
 109  $\text{In}_{0.5}\text{Ga}_{0.5}\text{P}$  were grown at a temperature of  $700\ ^\circ\text{C}$ , and the subsequent p-doped layers  
 110 were grown at  $660\ ^\circ\text{C}$ . At room temperature, the grown  $\text{In}_{0.5}\text{Ga}_{0.5}\text{P}$  had a  
 111 photoluminescence peak energy of  $1.89\ \text{eV}$ . This energy is in good agreement with the  
 112 bandgap of the material with a suppressed spontaneous long-range ordering in the group  
 113 III sublattice [17]. The Ohmic contact on top of the  $\text{p}^+$  GaAs layer was formed from Ti  
 114 (thickness of  $20\ \text{nm}$ ) and Au (thickness of  $200\ \text{nm}$ ). The Ohmic rear contact, deposited  
 115 onto the rear of the  $\text{n}^+$  GaAs substrate, was formed from InGe (thickness of  $20\ \text{nm}$ ) and  
 116 Au (thickness of  $200\ \text{nm}$ ). The  $\text{In}_{0.5}\text{Ga}_{0.5}\text{P}$  photodiode was not passivated. Chemical  
 117 wet etching techniques ( $1:1:1\ \text{K}_2\text{Cr}_2\text{O}_7:\text{HBr}:\text{CH}_3\text{COOH}$  solution followed by a  $10\ \text{s}$   
 118 finishing etch in  $1:8:80\ \text{H}_2\text{SO}_4:\text{H}_2\text{O}_2:\text{H}_2\text{O}$  solution) were used to fabricate the  $200\ \mu\text{m}$   
 119 diameter  $\text{In}_{0.5}\text{Ga}_{0.5}\text{P}$  mesa device used in the study. The device layers, their relative  
 120 thicknesses and materials are summarised in TABLE 1.

121

122 TABLE 1. Layer details of the  $\text{In}_{0.5}\text{Ga}_{0.5}\text{P}$  photodiode.

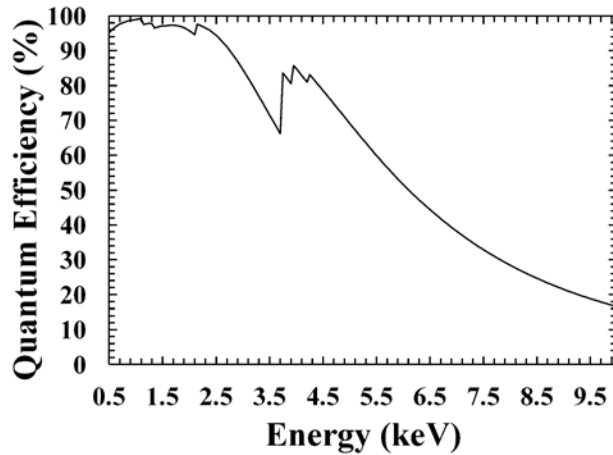
Layer	Material	Thickness ( $\mu\text{m}$ )	Dopant	Dopant Type	Doping density ( $\text{cm}^{-3}$ )
1	Ti	0.02			
2	Au	0.2			
3	GaAs	0.01	Zn	$\text{p}^+$	$1 \times 10^{19}$
4	$\text{In}_{0.5}\text{Ga}_{0.5}\text{P}$	0.2	Zn	$\text{p}^+$	$2 \times 10^{18}$
5	$\text{In}_{0.5}\text{Ga}_{0.5}\text{P}$	5	undoped		$< 5 \times 10^{16}$
6	$\text{In}_{0.5}\text{Ga}_{0.5}\text{P}$	0.1	Si	$\text{n}^+$	$2 \times 10^{18}$
7	GaAs buffer	0.3	Si	$\text{n}^+$	$2 \times 10^{18}$
8	Substrate $\text{n}^+$ GaAs	350	Si	$\text{n}^+$	$2 \times 10^{18}$
9	InGe	0.02			
10	Au	0.2			

123

124 A  $192\ \text{MBq}\ ^{55}\text{Fe}$  radioisotope X-ray source ( $\text{Mn}\ \text{K}\alpha = 5.9\ \text{keV}$ ,  $\text{Mn}\ \text{K}\beta = 6.49\ \text{keV}$ ) was  
 125 positioned  $5\ \text{mm}$  away from the top surface of the  $200\ \mu\text{m}$  diameter  $\text{In}_{0.5}\text{Ga}_{0.5}\text{P}$  mesa  
 126 photodiode such as to study the detector performances under illumination.

127

128 The  $\text{In}_{0.5}\text{Ga}_{0.5}\text{P}$  X-ray quantum efficiencies ( $QE$ ) through the device's optical window  
 129 (region not covered by contacts) were calculated using the Beer-Lambert law and  
 130 assuming complete charge collection in the p and i layers. Figure 1 shows the  
 131  $\text{In}_{0.5}\text{Ga}_{0.5}\text{P}$  X-ray quantum efficiencies as a function of photon energy up to 10 keV.  
 132



133  
 134 Figure 1. Calculated  $\text{In}_{0.5}\text{Ga}_{0.5}\text{P}$  X-ray quantum efficiencies as a function of photon  
 135 energy.  
 136

137 X-ray quantum efficiencies ( $QE$ ) of 53% at 5.9 keV and 44% at 6.49 keV were  
 138 computed for the structure. TABLE 2 shows the attenuation coefficients at 5.9 keV  
 139 and 6.49 keV for  $\text{In}_{0.5}\text{Ga}_{0.5}\text{P}$  as well as other different materials. The attenuation  
 140 coefficients for binary and ternary compounds were estimated from the attenuation  
 141 coefficients of their single elements, properly weighted [15, 16].  
 142

143 TABLE 2. Attenuation coefficients at 5.9 keV and 6.49 keV for different materials.

Material	Attenuation coefficient at 5.9 keV ( $\text{cm}^{-1}$ )	Attenuation coefficient at 6.49 keV ( $\text{cm}^{-1}$ )
$\text{In}_{0.5}\text{Ga}_{0.5}\text{P}$	1464	1130
$\text{Al}_{0.52}\text{In}_{0.48}\text{P}$	1301	1004
GaAs	837	642
$\text{Al}_{0.8}\text{Ga}_{0.2}\text{As}$	788	604
Si	346	263

144  
 145  $QE$  at 5.9 keV greater than 90% may be obtained by increasing the  $\text{In}_{0.5}\text{Ga}_{0.5}\text{P}$  i layer  
 146 thickness to 30  $\mu\text{m}$ ; this i layer thickness may be achieved in future  $\text{In}_{0.5}\text{Ga}_{0.5}\text{P}$   
 147 structures as consequence of advances in growth and fabrication technologies. Because  
 148 of the higher linear attenuation coefficients of  $\text{In}_{0.5}\text{Ga}_{0.5}\text{P}$  with respect to SiC, the

149 quantum efficiency of the 5  $\mu\text{m}$   $\text{In}_{0.5}\text{Ga}_{0.5}\text{P}$  device at high X-ray photon energies ( $> 48$   
150 keV) are expected to be higher than those of a 300  $\mu\text{m}$  SiC detector at the same energies.

151

## 152 **2.2 CHARACTERIZATION SETUP**

153

154 The  $\text{In}_{0.5}\text{Ga}_{0.5}\text{P}$  device was installed inside a TAS Micro MT climatic cabinet for  
155 temperature control. The temperature was initially set to 100  $^{\circ}\text{C}$  and decreased to 20  
156  $^{\circ}\text{C}$ , in steps of 20  $^{\circ}\text{C}$ . Before taking any measurements at each temperature, the device  
157 was left for 30 minutes to ensure stabilisation.

158

159 The  $\text{In}_{0.5}\text{Ga}_{0.5}\text{P}$  leakage current as a function of reverse bias was measured using a  
160 Keithley 6487 picoammeter/voltage source. The uncertainty associated with individual  
161 current readings was 0.3% of their values plus 400 fA, while the uncertainty associated  
162 with applied biases was 0.1% of their values plus 1 mV [18]. The  $\text{In}_{0.5}\text{Ga}_{0.5}\text{P}$   
163 capacitance as a function of reverse bias was measured using an HP 4275A Multi  
164 Frequency LCR meter. The uncertainty associated with each capacitance reading was  
165 0.12% [19], while the uncertainty associated with applied biases was 0.1% of their  
166 values plus 1 mV [18]. The test signal was sinusoidal with a 50 mV rms magnitude  
167 and 1 MHz frequency. In both leakage current and capacitance measurements, the  
168 reverse bias increased from 0 V to 15 V (in 1 V increments).

169

170 X-ray spectra were obtained using the  $^{55}\text{Fe}$  radioisotope X-ray source to illuminate the  
171 200  $\mu\text{m}$  diameter  $\text{In}_{0.5}\text{Ga}_{0.5}\text{P}$  device at temperatures from 100  $^{\circ}\text{C}$  to 20  $^{\circ}\text{C}$ . The  
172 experimental setup utilised a custom-made charge-sensitive preamplifier of feedback  
173 resistorless design, similar to that reported in ref. [20]. The preamplifier was operated  
174 at the same temperature as the photodiode. The signal from the preamplifier was  
175 shaped by an Ortec 572a shaping amplifier, and digitized by a multichannel analyser  
176 (Ortec Easy-MCA-8K). Spectra were accumulated and analysed at shaping times of  
177 0.5  $\mu\text{s}$ , 1  $\mu\text{s}$ , 2  $\mu\text{s}$ , 3  $\mu\text{s}$ , 6  $\mu\text{s}$ , and 10  $\mu\text{s}$ . The  $\text{In}_{0.5}\text{Ga}_{0.5}\text{P}$  device was reverse biased at 0  
178 V, 5 V, 10 V, and 15 V, in each case. The live time for each spectrum was 200 s.

179

180 All the experiments were performed in dry nitrogen atmosphere (relative humidity  
181  $<5\%$ ) as a precautionary measure to eliminate any formation of water vapor at high  
182 temperatures and water condensation at low temperatures inside the chamber.

183

### 184 3. RESULTS

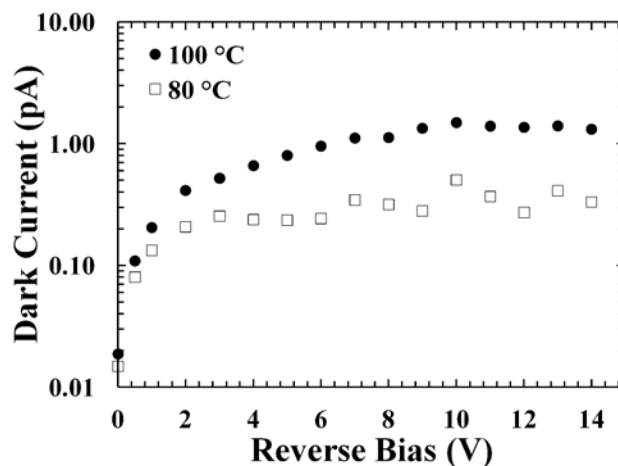
185

#### 186 3.1 Current and capacitance measurements

187

188 The measured leakage currents of the packaged device at 100 °C and 80 °C are shown  
189 in Figure 2; leakage currents at temperatures below 80 °C are not reported because they  
190 were below the picoammeter's noise floor. Measurements of the leakage current as a  
191 function of the reverse bias of the system when the diode was not connected showed  
192 that the system was contributing to the measured leakage current. At 100 °C and at 80  
193 °C, the packaged device (defined as the semiconductor and system combined) had  
194 leakage currents of 1.5 pA and 0.5 pA, respectively, at a reverse bias of 10 V. At the  
195 same temperatures and reverse bias condition, the system (with no diode connected)  
196 had leakage currents of 1.1 pA and 0.2 pA, respectively. When the reverse bias was  
197 increased to 15 V in each case, the leakage currents measured for the packaged device  
198 and the system became indistinguishable at both temperatures. Considering the  
199 uncertainties associated with the leakage current measurements, the leakage current  
200 from the diode itself can be considered negligible compared with the other leakage  
201 currents.

202



203

204 Figure 2. Leakage current of the packaged  $\text{In}_{0.5}\text{Ga}_{0.5}\text{P}$  detector (i.e. from both the  
205 semiconductor junction and the package) as a function of applied reverse bias at 100  
206 °C (filled circles) and 80 °C (empty squares).

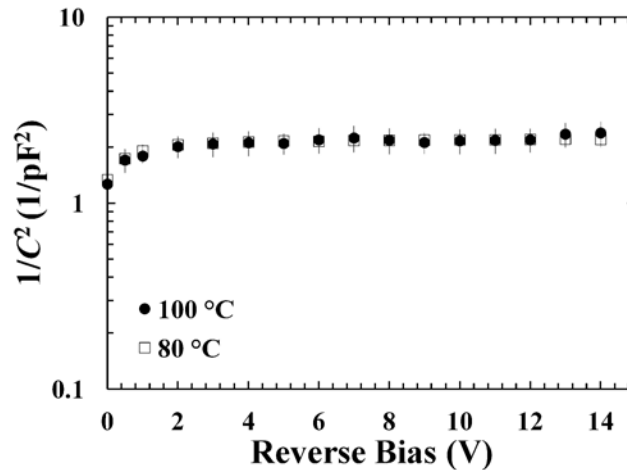
207

208

209 At different temperatures, the capacitance of the packaged  $\text{In}_{0.5}\text{Ga}_{0.5}\text{P}$  detector as a  
210 function of reverse bias was measured. The capacitance of an empty package of the  
211 same type was also measured at different temperatures and subtracted from the



212 measured capacitance of the packaged  $\text{In}_{0.5}\text{Ga}_{0.5}\text{P}$  photodiode. At each temperature,  
 213 the capacitances were measured multiple times; the mean and its relative root mean  
 214 squared (RMS) error were considered. The capacitances of the empty package were  
 215 measured to be  $1.27 \text{ pF} \pm 0.02 \text{ pF}$  and  $1.132 \text{ pF} \pm 0.003 \text{ pF}$  at  $100 \text{ }^\circ\text{C}$  and  $80 \text{ }^\circ\text{C}$ ,  
 216 respectively. The uncertainties reflect not only the uncertainty in one measurements,  
 217 but also the variation in measured value upon repetition; greater variation was seen at  
 218  $100 \text{ }^\circ\text{C}$  than at  $80 \text{ }^\circ\text{C}$ . In the temperature range studied, the capacitance of the  
 219  $\text{In}_{0.5}\text{Ga}_{0.5}\text{P}$  detector itself ( $C$ ) was found to be temperature invariant.  $1/C^2$  as a function  
 220 of reverse bias at  $100 \text{ }^\circ\text{C}$  and at  $80 \text{ }^\circ\text{C}$  is shown in Figure 3, similar results were found  
 221 at temperatures  $\leq 60 \text{ }^\circ\text{C}$ . A dependence between  $1/C^2$  and the reverse bias was found  
 222 at reverse biases below  $3 \text{ V}$ ;  $1/C^2$  was constant at reverse biases higher than  $3 \text{ V}$ .  
 223



224  
 225 Figure 3.  $1/C^2$  as a function of applied reverse bias. The temperatures analysed were  
 226  $100 \text{ }^\circ\text{C}$  (filled circles) and  $80 \text{ }^\circ\text{C}$  (empty squares).  
 227

228  
 229 **3.2 X-ray spectroscopy and noise analysis**  
 230

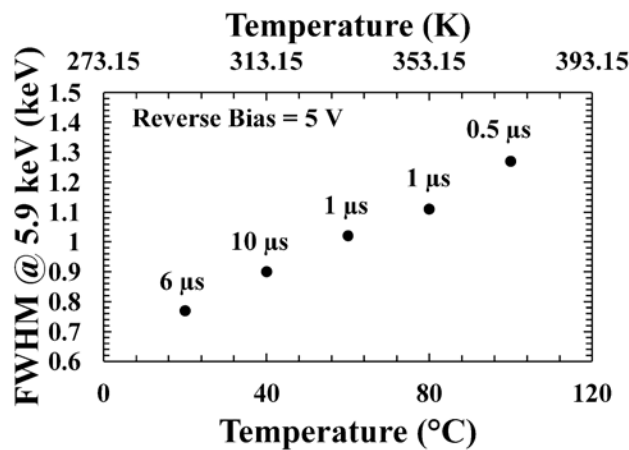
231 X-ray spectra were obtained using the  $^{55}\text{Fe}$  radioisotope X-ray source. Although  
 232 temperatures above  $100 \text{ }^\circ\text{C}$  can be achieved by the TAS Micro MT climatic cabinet,  
 233 temperatures higher than  $100 \text{ }^\circ\text{C}$  were not studied because of limitations in the working  
 234 temperature range of the spectrometer's electrical cables. At  $100 \text{ }^\circ\text{C}$ , the diode was  
 235 stable throughout the spectrum acquisition time. The diode did not degrade after being  
 236 used at such temperatures. Moreover, polarization phenomena were not observed in  
 237 the detector at any of the temperatures or biases studied.  
 238

239 An improvement in energy resolution (as quantified by the FWHM at 5.9 keV) was  
 240 observed when increasing the applied reverse bias from 0 V to 5 V. This result can be  
 241 explained considering the reduction in capacitance of the detector and possibly  
 242 improved charge collection. No further change in FWHM was observed when  
 243 operating the detector at reverse biases > 5 V. The latter behaviour can be explained  
 244 considering that the In<sub>0.5</sub>Ga<sub>0.5</sub>P photodiode is fully depleted above 5 V.

245

246 The optimum shaping time (i.e. that which produced the smallest FWHM) varied with  
 247 temperature, as shown in Figure 4. The FWHM decreased at lower temperatures  
 248 because of the lower leakage currents of the In<sub>0.5</sub>Ga<sub>0.5</sub>P photodiode and Si JFET at such  
 249 temperatures. The spectra with the best energy resolution (smallest FWHM) at 100 °C  
 250 and 20 °C with the photodiode reverse biased at 5 V are presented in Figure 5. The  
 251 observed <sup>55</sup>Fe photopeaks were the combination of the characteristic Mn K $\alpha$  (5.9 keV)  
 252 and Mn K $\beta$  (6.49 keV) lines of the <sup>55</sup>Fe radioisotope X-ray source. To determine the  
 253 FWHM of the 5.9 keV peaks in Figures 4 and 5, Gaussian fitting was performed on the  
 254 photopeaks: the Mn K $\alpha$  and Mn K $\beta$  peaks were deconvolved from detected combined  
 255 photopeak. The fitting took into account the relative X-ray emission rates of the <sup>55</sup>Fe  
 256 radioisotope X-ray source at 5.9 keV and 6.49 keV in the appropriate ratio [21] as well  
 257 as the relative efficiency of the detector at these X-ray energies.

258



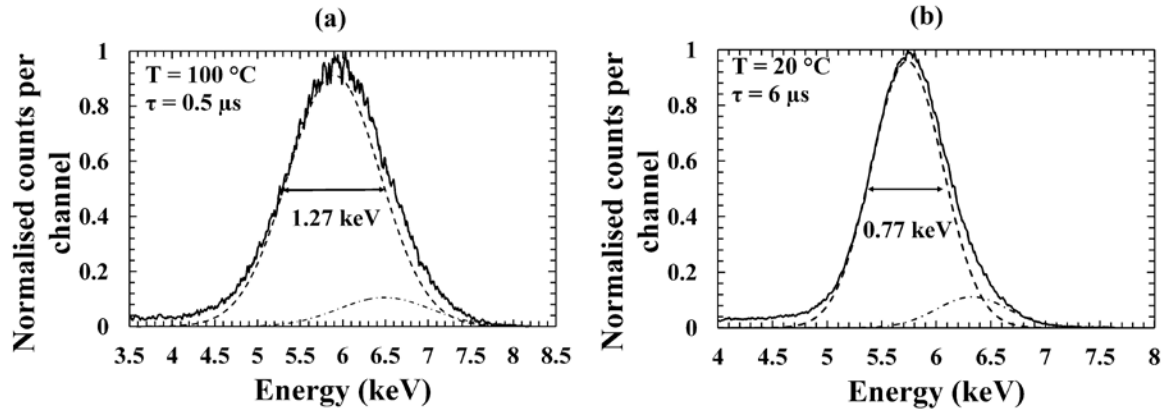
259

260 Figure 4. The smallest observed FWHM of the 5.9 keV peak as a function of  
 261 temperature at the optimum shaping time, when the In<sub>0.5</sub>Ga<sub>0.5</sub>P detector was reverse  
 262 biased at 5 V.

263

264

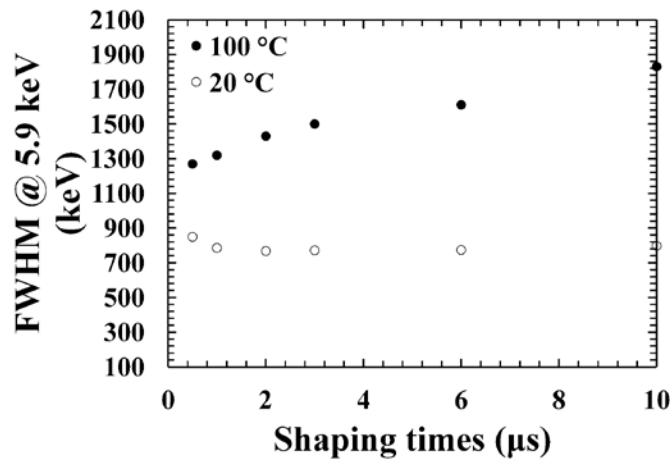
265



266  
267  
268  
269  
270  
271

Figure 5. Best energy resolution  $^{55}\text{Fe}$  X-ray spectra collected at 100 °C (a) and at 20 °C (b) with the  $\text{In}_{0.5}\text{Ga}_{0.5}\text{P}$  photodiode reverse biased at 5 V. Also shown in each spectrum are the deconvolved Mn  $K\alpha$  (dashed line) and Mn  $K\beta$  (dashed-dot line) peaks.

272 The FWHM of the 5.9 keV peak as a function of shaping time at 100 °C and 20 °C,  
273 with the photodiode reverse biased at 5 V, are presented in Figure 6.



274  
275  
276  
277  
278

Figure 6. FWHM of the 5.9 keV peak as a function of shaping time at 100 °C (filled circles) and 20 °C (empty circles), when the  $\text{In}_{0.5}\text{Ga}_{0.5}\text{P}$  detector was reverse biased at 5 V.

279 The energy resolution (FWHM) of a non-avalanche X-ray photodiode spectrometer is  
280 degraded by the Fano noise, the charge trapping noise, and the electronic noise [22, 23].  
281 The Fano noise is due to the statistical nature of the ionisation process; it is calculated  
282 and explained in section “C. Fano-limited energy resolution and electron-hole pair  
283 creation energy”. At each temperature studied, the observed FWHM was greater than  
284 the expected Fano limited energy resolution, indicating that noise sources other than  
285 the statistical charge creation process were significant. In a photodiode X-ray  
286 spectrometer, the electronic noise is caused by 5 different components: parallel white

287 noise, series white noise, induced gate current noise,  $1/f$  noise, and dielectric noise [22,  
 288 23]. The leakage currents of the detector and the Si input JFET of the preamplifier  
 289 (which was operated uncooled at each temperature) influenced the parallel white noise,  
 290 as shown in equation 1 [22, 23, 24]. The capacitances of the detector and input JFET  
 291 of the preamplifier influence the series white noise and  $1/f$  noise, as shown in equations  
 292 2 and 3 [22, 23, 24]. Parallel white noise and series white noise are, respectively,  
 293 directly and inversely proportional to the shaping time; whilst  $1/f$  noise and dielectric  
 294 noise are independent of shaping time [22, 23].

295

$$296 \quad ENC_{wp} = \frac{1}{q} \sqrt{\frac{A_3}{2} 2q(I_D + I_{JFET})\tau} \quad (1)$$

$$297 \quad ENC_{ws} = \frac{B}{q} \sqrt{\frac{A_1}{2} 4kT \frac{\gamma}{g_m} (C_D + C_{JFET})^2 \frac{1}{\tau}} \quad (2)$$

$$298 \quad ENC_{1/f} = \frac{1}{q} \sqrt{A_2 \pi \gamma 4kT \frac{f_c}{g_m} (C_D + C_{JFET})^2} \quad (3)$$

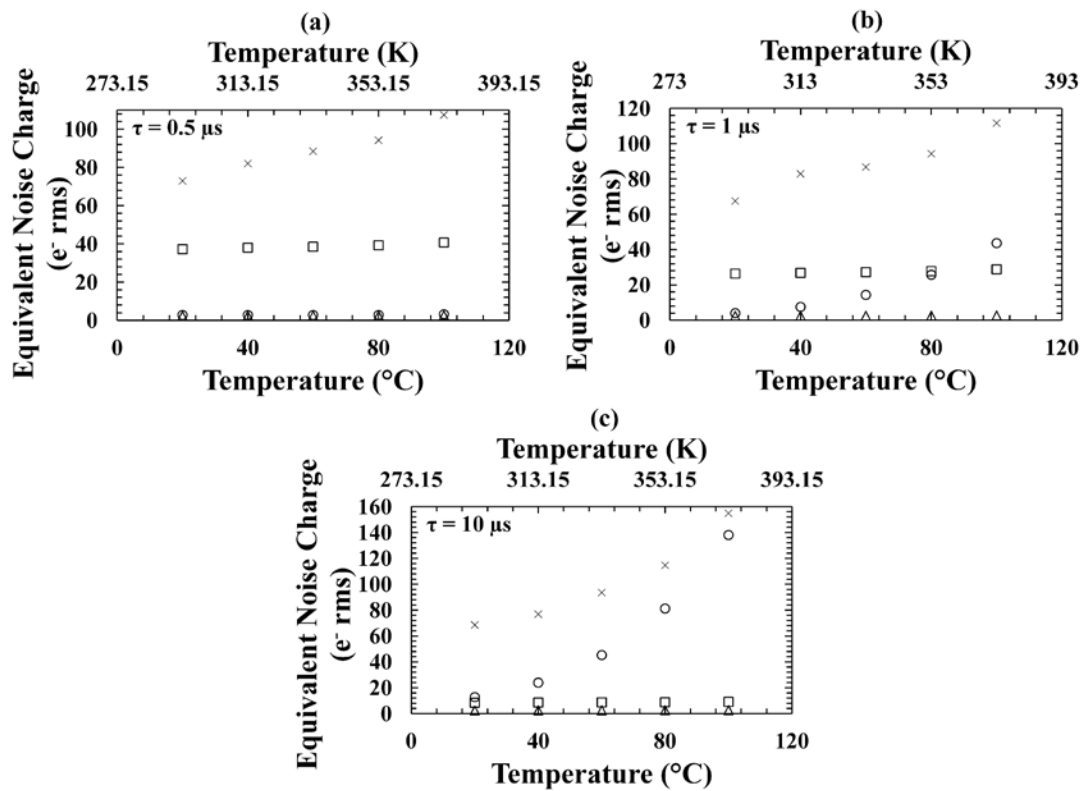
299

300 where  $A_1$ ,  $A_2$  and  $A_3$  are 1.85, 1.8, and 1.85, respectively [24];  $I_D$  the experimentally  
 301 measured packaged device leakage current at different temperatures,  $I_{JFET}$  the JFET  
 302 leakage current at different temperatures (at 20 °C the leakage current of the JFET was  
 303 1 pA);  $C_D$  the experimentally measured packaged device capacitance at different  
 304 temperatures,  $C_{JFET}$  the JFET capacitance (assumed to be 2 pF at all the temperatures  
 305 studied),  $g_m$  the JFET transconductance (assumed to be 6 mS at the operating condition  
 306 of the JFET),  $\gamma$  the product of the noise resistance and the transconductance of the JFET  
 307 (0.85),  $B$  the induced gate current correction (0.8)[23],  $f_c$  the corner frequency of the  
 308 JFET (assumed to be 1000 Hz at the operating condition of the JFET) [25].

309

310 The obtained parallel white noise, series white noise (adjusted for induced gate current  
 311 noise [22, 23, 24], and  $1/f$  noise, as well as the measured equivalent noise charge, at  
 312 shaping times of (a) 0.5  $\mu$ s, (b) 1  $\mu$ s, and (c) 10  $\mu$ s, with the In<sub>0.5</sub>Ga<sub>0.5</sub>P photodiode  
 313 reverse biased at 5 V, are shown in Figure 7. In Figure 7 the measured equivalent noise  
 314 charge was calculated using the value of the In<sub>0.5</sub>Ga<sub>0.5</sub>P electron-hole pair creation  
 315 energy as determined at each temperature in section “3.3. Fano-limited energy  
 316 resolution and electron-hole pair creation energy”.

317



318

319 Figure 7. Equivalent noise charge as a function of temperature at shaping time of (a)  
 320  $0.5 \mu\text{s}$ , (b)  $1 \mu\text{s}$ , and (c)  $10 \mu\text{s}$ , when the  $\text{In}_{0.5}\text{Ga}_{0.5}\text{P}$  photodiode was reverse biased at 5  
 321 V. The graphs show the contributions of the parallel white noise (empty circles), the  
 322 series white noise (empty squares) and the  $1/f$  noise (empty triangles), as well as the  
 323 measured equivalent noise charge (crosses).

324

325 The high parallel white noise observed at increased temperatures and at increased  
 326 shaping times is not due to the high leakage current of the  $\text{In}_{0.5}\text{Ga}_{0.5}\text{P}$  detector, but  
 327 instead due to the higher current of the uncooled Si input JFET of the preamplifier [22].

328

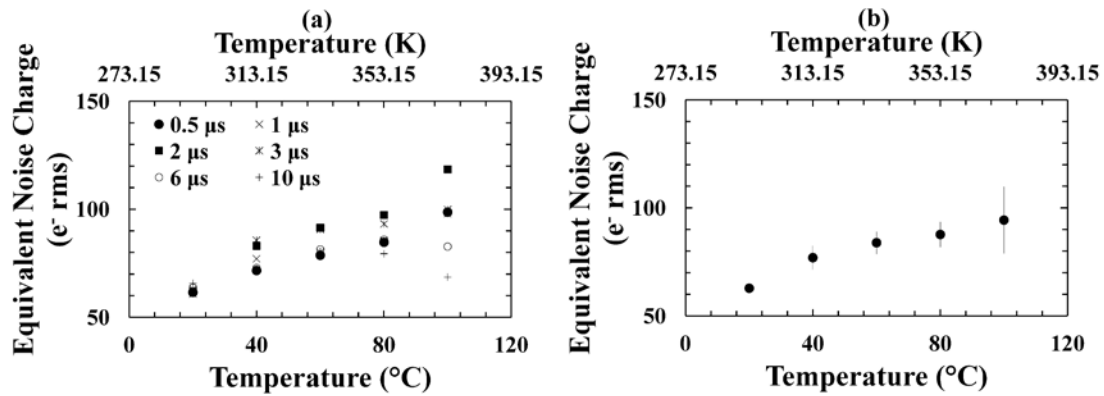
329 The FWHM of the 5.9 keV peak as a function of shaping time, reported in Figure 6,  
 330 shows that at  $100 \text{ }^\circ\text{C}$  the noise was leakage current limited, as expected when  
 331 combining in quadrature the parallel white noise and the series white noise of Figure 7.

332 Therefore, the shortest shaping time ( $0.5 \mu\text{s}$ ) gave the best energy resolution. The noise  
 333 at  $20 \text{ }^\circ\text{C}$  was not leakage current limited, as suggested by the FWHM of the 5.9 keV  
 334 peak as a function of shaping time (Figure 6). Thus, a long shaping time,  $6 \mu\text{s}$ , resulted  
 335 in the best energy resolution.

336

337 The temperature dependence of the residual noise is shown in Figure 8. At each shaping  
 338 time, the residual noise was estimated by subtracting in quadrature the known noise  
 339 components from the measured ENC. In Figure 8a, the residual noise dependence on

340 the temperature at all the six studied shaping times was reported. In Figure 8b, the  
 341 mean of the residual noises among the six shaping times (at each point the root mean  
 342 squared error was associated) as a function of temperature is shown. The measured  
 343 FWHM was converted into ENC using the values of the electron-hole pair creation  
 344 energies at each temperature as determined in section “3.3. Fano-limited energy  
 345 resolution and electron-hole pair creation energy”.



346  
 347 Figure 8. (a) Equivalent noise charge of the residual noise at 5.9 keV at each shaping  
 348 time studied as a function of temperature, when the  $\text{In}_{0.5}\text{Ga}_{0.5}\text{P}$  photodiode was reverse  
 349 biased at 5 V. (b) Mean of the equivalent noise charge of the residual noise at 5.9 keV  
 350 among the six shaping times as a function of temperature (at each point the root mean  
 351 squared error was associated), when the  $\text{In}_{0.5}\text{Ga}_{0.5}\text{P}$  photodiode was reverse biased at 5  
 352 V.  
 353

354 In the temperature range 100  $^{\circ}\text{C}$  to 20  $^{\circ}\text{C}$ , the residual noise contribution at 5.9 keV  
 355 linearly decreased with decreasing temperature: at 100  $^{\circ}\text{C}$  a value of  $94 e^- \text{ rms} \pm 15 e^-$   
 356 rms was calculated; whilst at 20  $^{\circ}\text{C}$  a value of  $63 e^- \text{ rms} \pm 2 e^- \text{ rms}$  was determined.

357  
 358 The  $\text{In}_{0.5}\text{Ga}_{0.5}\text{P}$  spectrometer allowed high temperature operation (up to the maximum  
 359 investigated, 100  $^{\circ}\text{C}$ ). It presented better FWHM than was achieved using  $\text{Al}_{0.52}\text{In}_{0.48}\text{P}$   
 360 [5] and  $\text{Al}_{0.8}\text{Ga}_{0.2}\text{As}$  [3] spectrometers, but not as good as has been demonstrated using  
 361 SiC detectors with lower noise readout electronics [4], at the same temperatures. It  
 362 should also be noted that the use of ultra-low-noise readout electronics, such as those  
 363 reported in Ref. [26] would likely improve the energy resolution achieved.

364  
 365 The ability to work at such high (100  $^{\circ}\text{C}$ ) temperatures together with their greater X-  
 366 ray attenuation coefficients makes  $\text{In}_{0.5}\text{Ga}_{0.5}\text{P}$  spectrometers preferred over recently  
 367 reported GaAs spectrometers which have a maximum operating temperature of 60  $^{\circ}\text{C}$   
 368 [2]. However, at more modest temperatures (e.g. 60  $^{\circ}\text{C}$ ) the previously reported GaAs

369 spectrometer had a better FWHM at 5.9 keV (840 eV) than the  $\text{In}_{0.5}\text{Ga}_{0.5}\text{P}$  spectrometer  
370 (1.02 keV). The presently reported  $\text{In}_{0.5}\text{Ga}_{0.5}\text{P}$  X-ray spectrometer also performed  
371 better at 100 °C than the previously reported  $\text{Al}_{0.52}\text{In}_{0.48}\text{P}$  X-ray spectrometer. The  
372 FWHM at 5.9 keV for the  $\text{In}_{0.5}\text{Ga}_{0.5}\text{P}$  device was 1.27 keV at 100 °C c.f. 1.57 keV for  
373 the  $\text{Al}_{0.52}\text{In}_{0.48}\text{P}$  device using similar device readout electronics.  $\text{In}_{0.5}\text{Ga}_{0.5}\text{P}$  also has  
374 larger linear attenuation coefficients than  $\text{Al}_{0.52}\text{In}_{0.48}\text{P}$ .

375

376 Since the readout electronics used to characterise these materials have been broadly  
377 comparable, the difference in obtained FWHM for these materials (GaAs, AlInP,  
378 InGaP) can be explained considering their different electron-hole pair creation energies  
379 and the noise contributions of the readout electronics at high temperature (see section  
380 “3.3 Fano-limited energy resolution and electron-hole pair creation energy”). A total  
381 noise at the input of the preamplifier of 86 e<sup>-</sup> rms, for example, corresponds to 840 eV  
382 in GaAs, to 1.00 keV in  $\text{In}_{0.5}\text{Ga}_{0.5}\text{P}$  and to 1.08 keV in  $\text{Al}_{0.52}\text{In}_{0.48}\text{P}$ . The observed  
383 FWHM of 1.02 keV at 5.9 keV at 60 °C for the  $\text{In}_{0.5}\text{Ga}_{0.5}\text{P}$  spectrometer was very close  
384 to the expected value. Therefore, the total noise in e<sup>-</sup> rms was similar in the GaAs and  
385  $\text{In}_{0.5}\text{Ga}_{0.5}\text{P}$  spectrometers, since the preamplifier was limited by noises other than the  
386 detector leakage current at these temperatures.

387

388 However, the energy resolution achieved with the very best SiC X-ray detectors  
389 coupled to much lower noise readout electronics [4] is superior to that obtained with  
390  $\text{In}_{0.5}\text{Ga}_{0.5}\text{P}$  and our preamplifier electronics. A SiC detector with FWHM of 233 eV at  
391 5.9 keV has been reported at 100 °C [4]. It would be interesting to characterise the  
392  $\text{In}_{0.5}\text{Ga}_{0.5}\text{P}$  detectors with the same ultra-low noise electronics used for the SiC  
393 detectors to establish a better comparison between the materials. It should also be noted  
394 that the X-ray attenuation coefficients of  $\text{In}_{0.5}\text{Ga}_{0.5}\text{P}$  are much greater than those for  
395 SiC. Thus, even if the ultimately achievable energy resolution with  $\text{In}_{0.5}\text{Ga}_{0.5}\text{P}$  is more  
396 modest than SiC,  $\text{In}_{0.5}\text{Ga}_{0.5}\text{P}$  may still be preferred for low-flux, high-energy  
397 applications.

398

### 399 **3.3 Fano-limited energy resolution and electron-hole pair creation energy**

400

401 The Fano-limited energy resolution is related to the charge creation process at the  
402 absorption of an X-ray photon, and is the statistically limited energy resolution of a

403 non-avalanche X-ray photodiode spectrometer [27]. The Fano-limited energy  
 404 resolution (FWHM in eV) can be calculated using equation 4:

405

$$406 \quad FWHM = 2.35\varepsilon \sqrt{\frac{FE}{\varepsilon}} \quad (4)$$

407

408 where  $\varepsilon$  is the semiconductor electron-hole pair creation energy,  $F$  is the Fano factor,  
 409 and  $E$  is the X-ray photon's energy. Different semiconductors have different Fano  
 410 limited energy resolutions at the same X-ray photon's energy. This is because the Fano  
 411 limited energy resolution at each energy is dependent on physical material properties  
 412 (average electron-hole pair creation energy and Fano factor).

413

414 For the room temperature (20 °C) measurements of the electron-hole pair creation  
 415 energy, a method similar to that reported by other researchers [28, 29, 30, 31] was used.  
 416 The charge created by the absorption of X-rays from the  $^{55}\text{Fe}$  radioisotope X-ray source  
 417 in the  $\text{In}_{0.5}\text{Ga}_{0.5}\text{P}$  photodiode was measured relative to that created in a reference 200  
 418  $\mu\text{m}$  GaAs mesa photodiode. The structure of the GaAs device is summarised in TABLE  
 419 3. The  $\text{In}_{0.5}\text{Ga}_{0.5}\text{P}$  and GaAs detectors were connected in parallel to the custom-made  
 420 low-noise charge-sensitive preamplifier.

421

422 TABLE 3. Layer details of the GaAs photodiode.

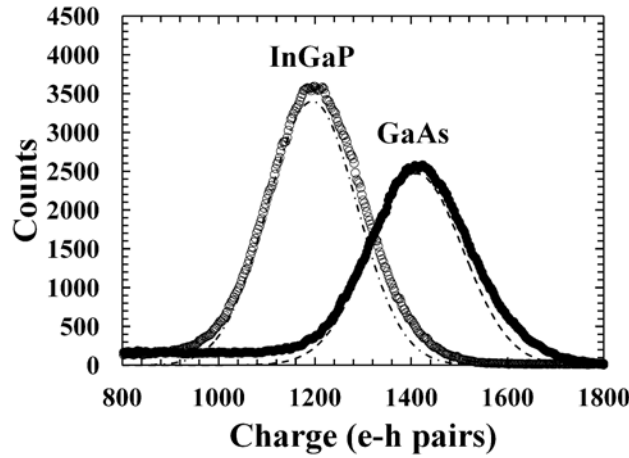
Layer	Material	Thickness ( $\mu\text{m}$ )	Dopant	Dopant Type	Doping density ( $\text{cm}^{-3}$ )
1	Ti	0.02			
2	Au	0.2			
3	GaAs	0.5	Be	p <sup>+</sup>	$2 \times 10^{18}$
4	GaAs	10	undoped		$< 10^{15}$
5	GaAs	1	Si	n <sup>+</sup>	$2 \times 10^{18}$
6	Substrate n <sup>+</sup> GaAs				
7	InGe	0.02			
8	Au	0.2			

423

424 The  $\text{In}_{0.5}\text{Ga}_{0.5}\text{P}$  and the GaAs photodetectors were both independently reverse biased  
 425 at 10 V. Spectra were accumulated with the  $^{55}\text{Fe}$  radioisotope X-ray source illuminating  
 426 the  $\text{In}_{0.5}\text{Ga}_{0.5}\text{P}$  device and the GaAs device separately, in turn. Gaussians were fitted  
 427 to the detected Mn K $\alpha$  (5.9 keV) and Mn K $\beta$  (6.49 keV) peaks of the accumulated



428 spectra; the  $^{55}\text{Fe}$  X-ray spectra accumulated and the fitted 5.9 keV peaks for the  
 429  $\text{In}_{0.5}\text{Ga}_{0.5}\text{P}$  detector and the GaAs reference photodetector are shown in Figure 9.  
 430



431  
 432 Figure 9.  $^{55}\text{Fe}$  X-ray spectra accumulated at 10 V reverse bias using the  $\text{In}_{0.5}\text{Ga}_{0.5}\text{P}$   
 433 device (empty circles) and the GaAs reference photodetector (filled circles) under the  
 434 illumination of  $^{55}\text{Fe}$  radioisotope X-ray source. Also shown are the fitted 5.9 keV lines  
 435 for the  $\text{In}_{0.5}\text{Ga}_{0.5}\text{P}$  device (dashed-dot line) and the GaAs reference photodetector  
 436 (dashed line). For clarity, the fitted 6.49 keV Mn  $\text{K}\beta$  peaks are not shown but were  
 437 included appropriately in the fitting.  
 438

439 The quantity of charge corresponding to each MCA channel was calculated using the  
 440 position of the zero noise energy peak of the preamplifier and the 5.9 keV peak detected  
 441 by the GaAs reference photodiode. In this calculation, the GaAs electron-hole pair  
 442 creation energy,  $4.184 \text{ eV} \pm 0.025 \text{ eV}$ , [28] was also used. The  $\text{In}_{0.5}\text{Ga}_{0.5}\text{P}$  electron-  
 443 hole pair creation energy ( $\epsilon_{\text{InGaP}}$ ) was then determined using equation 5:

444

$$445 \quad \epsilon_{\text{InGaP}} = \epsilon_{\text{GaAs}} \left( \frac{N_{\text{GaAs}}}{N_{\text{InGaP}}} \right) \quad (5)$$

446

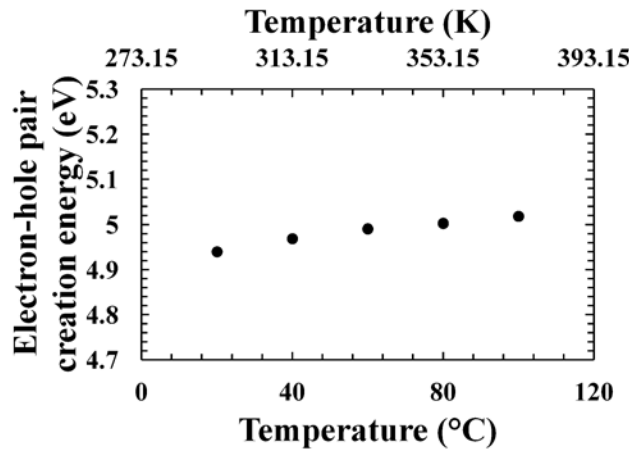
447 where  $\epsilon_{\text{GaAs}}$  is the electron-hole pair creation energy in GaAs,  $N_{\text{GaAs}}$  and  $N_{\text{InGaP}}$  are the  
 448 number of charges created in the GaAs reference detector and  $\text{In}_{0.5}\text{Ga}_{0.5}\text{P}$  detector,  
 449 respectively. An experimental value of  $4.94 \text{ eV} \pm 0.06 \text{ eV}$  was measured for  $\epsilon_{\text{InGaP}}$  at  
 450 room temperature ( $20 \text{ }^\circ\text{C}$ ). To examine the effect of operating the  $\text{In}_{0.5}\text{Ga}_{0.5}\text{P}$  detector  
 451 at higher reverse biases, the reverse bias was increased to 15 V, and the experiment  
 452 repeated. An electron-hole pair creation energy of  $4.90 \text{ eV} \pm 0.04 \text{ eV}$  was measured in  
 453 this instance. The similarity of the values further confirms that charge trapping was  
 454 negligible. If charge trapping was significant, a substantial reduction in apparent

455 electron-hole pair creation energy would have been observed at higher reverse bias as  
456 a consequence of the improved charge transport at higher electric field.

457

458 The dependence of the  $\text{In}_{0.5}\text{Ga}_{0.5}\text{P}$  electron-hole pair creation energy upon temperature  
459 was studied across the temperature range 100 °C to 20 °C. For this set of measurements,  
460 the  $\text{In}_{0.5}\text{Ga}_{0.5}\text{P}$  detector was individually connected to the custom-made low-noise  
461 charge-sensitive preamplifier (i.e. without the GaAs reference detector) and illuminated  
462 by the  $^{55}\text{Fe}$  radioisotope X-ray source. The change in conversion factor of the  
463 preamplifier itself with temperature was measured across the temperature range by  
464 connecting a stabilized pulse generator (Berkeley Nucleonics Corporation model BH-  
465 1) to the test signal input of the preamplifier. The change in position of the centroid of  
466 the pulse generator peak allowed the change in performance of the preamplifier with  
467 temperature to be untangled from the change in electron-hole pair creation energy of  
468 the photodiode. The change in position of the centroid of the pulse generator peak was  
469 appropriately corrected for the change in the test capacitance with temperature [32].  
470 Spectra were collected and Gaussians were fitted to the photopeak and the peak from  
471 the pulse generator in order to determine the positions of their centroids with respect to  
472 the zero noise peak. The charge created in the  $\text{In}_{0.5}\text{Ga}_{0.5}\text{P}$  photodiode by the X-ray  
473 photons was related to the relative change in position of the photopeak on the MCA's  
474 charge scale. The latter was corrected for the preamplifier's change in conversion  
475 factor with temperature (determined from the pulser peak) [31, 33]. The different  
476 quantities of charge created at different temperatures was caused by the change in the  
477  $\text{In}_{0.5}\text{Ga}_{0.5}\text{P}$  electron-hole pair creation energy ( $\epsilon_{\text{InGaP}}$ ). At each temperature, the  
478 absolute value of  $\epsilon_{\text{InGaP}}$  was then computed using the previously determined room  
479 temperature  $\epsilon_{\text{InGaP}}$ . The apparent  $\text{In}_{0.5}\text{Ga}_{0.5}\text{P}$  electron-hole pair creation energy as a  
480 function of temperature is reported in Figure 10. The uncertainties associated with the  
481 electron-hole pair creation energy values were obtained by propagating the uncertainty  
482 in the electron-hole pair creation energy at room temperature and the uncertainty in the  
483 relative change in the conversion factors. The uncertainty in the electron-hole pair  
484 creation energy at room temperature ( $\pm 0.06$  eV) was an order of magnitude greater  
485 than the uncertainties in the relative change in the conversion factors ( $\pm 0.005$  eV);  
486 therefore, the former mainly affected the uncertainties in the electron-hole pair creation  
487 energy at different temperatures. A similar experimental setup was used by other

488 researchers to measure the electron-hole pair creation energy in other materials [31,  
 489 33].  
 490



491  
 492 Figure 10. Temperature dependence of the energy consumed to produce an electron-  
 493 hole pair in  $\text{In}_{0.5}\text{Ga}_{0.5}\text{P}$ .  
 494

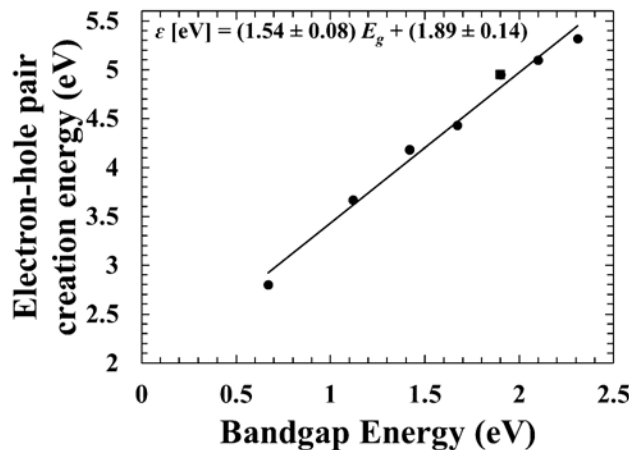
495 An apparent slight trend suggesting that the  $\text{In}_{0.5}\text{Ga}_{0.5}\text{P}$  electron-hole pair creation  
 496 energy increased with increasing temperature was found: at 100 °C,  $\epsilon_{\text{InGaP}} = 5.02 \text{ eV} \pm$   
 497  $0.07 \text{ eV}$ , whereas at 20 °C  $\epsilon_{\text{InGaP}} = 4.94 \text{ eV} \pm 0.06 \text{ eV}$ . However, the data points were  
 498 all within the uncertainties of each other for the temperature range investigated. If the  
 499 trend (greater average electron-hole pair creation energy at higher temperatures) was  
 500 real, the results would be surprising. It is conventionally considered that the average  
 501 electron-hole pair creation energy decreases linearly as the temperature increases [28,  
 502 31, 33, 34, 35]. Such a decrease can be understood considering the dependence of the  
 503 electron-hole pair creation energy on the material bandgap energy. According to Klein  
 504 [36], the empirical relationship between the electron-hole pair creation energy and the  
 505 bandgap energy in a semiconductor is linear. Since the bandgap decreases at increased  
 506 temperatures, a similar behaviour is expected for the electron-hole pair creation energy,  
 507 due at least in part to the change in bandgap. Theoretical Monte Carlo calculations  
 508 conducted by Fraser et al. [34] for silicon predicted the decrease of the Si electron-hole  
 509 pair creation energy as a function of temperature.  
 510

511 The expected Fano limited energy resolution (FWHM) at 5.9 keV of X-ray detectors  
 512 made from  $\text{In}_{0.5}\text{Ga}_{0.5}\text{P}$  was estimated using equation 4 and the determined values for  
 513 the electron-hole pair creation energy. The Fano factor for  $\text{In}_{0.5}\text{Ga}_{0.5}\text{P}$  has not yet been

514 measured, but assuming a Fano factor of 0.12 (as for GaAs [37]), the Fano limited  
 515 energy resolution would be expected to be 139 eV at 5.9 keV at 20 °C. If the Fano  
 516 factor was 0.099 (as for CdZnTe [38]) a Fano limited energy resolution of 127 eV at  
 517 5.9 keV would be expected at 20 °C. Negligible changes over the 20 °C to 100 °C  
 518 temperature range were observed.

519

520 The electron-hole pair creation energy at 27 °C (300 K), which was interpolated from  
 521 the experimental measurements at 20 °C (293 K) and 40 °C (313 K), equalled 4.95 eV  
 522  $\pm$  0.07 eV. This is in agreement with the value predicted for In<sub>0.5</sub>Ga<sub>0.5</sub>P (4.83 eV  $\pm$   
 523 0.21 eV) by the empirical Bertuccio-Maiocchi-Barnett (BMB) relationship [31]. Figure  
 524 11 shows the average electron-hole pair creation energy for Ge, Si, GaAs, Al<sub>0.2</sub>Ga<sub>0.8</sub>As,  
 525 Al<sub>0.8</sub>Ga<sub>0.2</sub>As, Al<sub>0.52</sub>In<sub>0.48</sub>P [39], and In<sub>0.5</sub>Ga<sub>0.5</sub>P, and as a function of their respective  
 526 bandgap energies, at a temperature of 300 K.



527

528 Figure 11. Electron-hole pair creation energy for Ge, Si, GaAs, Al<sub>0.2</sub>Ga<sub>0.8</sub>As,  
 529 Al<sub>0.8</sub>Ga<sub>0.2</sub>As, and Al<sub>0.52</sub>In<sub>0.48</sub>P (filled circles), and In<sub>0.5</sub>Ga<sub>0.5</sub>P (filled square), as a  
 530 function of their bandgap energy at 300 K. The equation shown for the relationship has  
 531 been refined using the new data for In<sub>0.5</sub>Ga<sub>0.5</sub>P.  
 532

533 A linear least squares fit of the data showed that the previously reported BMB  
 534 dependence between electron-hole pair creation energy and bandgap energy can be  
 535 refined using the new data for In<sub>0.5</sub>Ga<sub>0.5</sub>P. The new relation is  $\epsilon = AE_g + B$  with  $A =$   
 536  $(1.54 \pm 0.08)$  and  $B = 1.89 \text{ eV} \pm 0.14 \text{ eV}$ . Using this relationship, the  $\epsilon_{InGaP}$  would be  
 537 expected to be  $4.82 \text{ eV} \pm 0.3 \text{ eV}$ .

538

539 As is the case for Al<sub>0.8</sub>Ga<sub>0.2</sub>As [30, 33] and Al<sub>0.2</sub>Ga<sub>0.8</sub>As [31], the electron-hole pair  
 540 creation energy value reported here at 300 K for In<sub>0.5</sub>Ga<sub>0.5</sub>P does not lie either on the

541 main or secondary Klein function branches [1, 36]. If  $\text{In}_{0.5}\text{Ga}_{0.5}\text{P}$  was on the main  
542 Klein function branch, the expected  $\epsilon_{\text{InGaP}}$  would be 6.17 eV, which is substantially  
543 higher than that found here ( $4.95 \text{ eV} \pm 0.03 \text{ eV}$ ). If it was on the secondary Klein  
544 function branch, the expected  $\epsilon_{\text{InGaP}}$  would be 4.07 eV, which is substantially lower  
545 than the obtained value. This lends further weight to the view that the Klein relationship  
546 is incomplete [31].

547

#### 548 **4. CONCLUSIONS**

549

550 For the first time an X-ray spectrometer with an InGaP detector was demonstrated  
551 across the temperature range 100 °C to 20 °C. The spectrometer was characterised at  
552 different shaping times and detector reverse biases. The best energy resolution  
553 (smallest FWHM) at 5.9 keV was 1.27 keV at 100 °C using a shaping time of 0.5  $\mu\text{s}$ ,  
554 this improved to 770 eV at 20 °C (using a shaping time of 6  $\mu\text{s}$ ), when the  $\text{In}_{0.5}\text{Ga}_{0.5}\text{P}$   
555 detector was reverse biased at 5 V. An improvement in energy resolution (as quantified  
556 by the FWHM at 5.9 keV) was observed when increasing the applied reverse bias from  
557 0 V to 5 V. The better results obtained at 5 V can be explained considering the  
558 improved charge collection in the greater electric field strength. Similar FWHM to that  
559 measured at 5 V were observed at 10 V and 15 V, suggesting that charge trapping noise  
560 at 5 V and above was negligible. System noise analysis showed that the observed  
561 FWHM were higher than the likely statistically limited energy resolution (i.e. the Fano-  
562 limited energy resolution). The parallel white noise, series white noise,  $1/f$  noise, and  
563 residual noise were calculated. The higher parallel white noise observed at increased  
564 temperatures was caused by the Si input JFET of the preamplifier rather than the  
565 photodetector. At 100 °C and at 0.5  $\mu\text{s}$ , for example, parallel white noises of 30.8  $e^-$   
566 rms for the Si JFET and 2.8  $e^-$  rms for the  $\text{In}_{0.5}\text{Ga}_{0.5}\text{P}$  device were found when the diode  
567 was reversed bias at 15 V. A dedicated experiment was conducted to measure the  
568  $\text{In}_{0.5}\text{Ga}_{0.5}\text{P}$  average electron-hole pair creation energy ( $\epsilon_{\text{InGaP}}$ ) in the temperature range  
569 100 °C to 20 °C.  $\epsilon_{\text{InGaP}}$  was found to be  $4.94 \text{ eV} \pm 0.06 \text{ eV}$  at 20 °C and  $5.02 \text{ eV} \pm 0.07$   
570  $\text{eV}$  at 100 °C.

571

#### 572 **ACKNOWLEDGMENTS**

573

574 This work was supported by STFC grants ST/M004635/1 and ST/P001815/1  
575 (University of Sussex, A. M. B., PI). A. M. B. acknowledges funding from the

576 Leverhulme Trust in the form of a 2016 Philip Leverhulme Prize. The authors are  
577 grateful to B. Harrison for growth of the GaAs structure, and R. J. Airey and S. Kumar  
578 for device fabrication and processing at the EPSRC National Epitaxy Facility for  
579 material growth and device fabrication.

580

## 581 REFERENCES

582

583 <sup>1</sup>A. Owens, A. Peacock, Nucl. Instrum. Meth. Phys. Res. A 531 (2004) 18.

584

585 <sup>2</sup>G. Lioliou, X. Meng, J. S. Ng, A. M. Barnett, Nucl. Instrum. Meth. Phys. Res., Sect.  
586 A 813 (2016) 1.

587

588 <sup>3</sup>A. M. Barnett, J. E. Lees, D. J. Bassford, J. S. Ng, C. H. Tan, N. Babazadeh, R. B.  
589 Gomes, Nucl. Instrum. Meth. Phys. Res., Sect. A 654 (2011) 336.

590

591 <sup>4</sup>G. Bertuccio, S. Caccia, D. Puglisi, D. Macera, Nucl. Instrum. Meth. Phys. Res., Sect.  
592 A 652 (2010) 193.

593

594 <sup>5</sup>S. Butera, T. Gohil, G. Lioliou, A. B. Krysa, A. M. Barnett, J. Appl. Phys 120 (2016)  
595 174503.

596

597 <sup>6</sup>M. R. Squillante, G. Entine Nucl. Instrum. Meth. Phys. Res. A 380 (1996) 160.

598

599 <sup>7</sup>S. U. Egariyev, K. T. Chen, A. Burger, R. B. James, C. M. Lisse, J. X-ray Sci.  
600 Technol. 6 (1996) 309.

601

602 <sup>8</sup>A. Zappettini, D. Macera, G. Benassi, N. Zambelli, D. Calestani, M.  
603 Ahangarianabhari, Y. Shi, G. Rotondo, B. Garavelli, P. Pozzi, G. Bertuccio, IEEE  
604 Nuclear Science Symposium and Medical Imaging Conference (NSS/MIC) (Seattle,  
605 WA, 8-15 November 2014).

606

607 <sup>9</sup>L. Abbene, G. Gerardi, G. Raso, F. Principato, N. Zambelli, G. Benassi, M. Bettelli,  
608 A. Zappettini, J. Synchrotron Rad. 24 (2017) 429.

609

610 <sup>10</sup>S. Butera, G. Lioliou, A. B. Krysa, A. M. Barnett, Sci. Rep. 7 (2017) 10206.

611

612 <sup>11</sup>A. Owens, Compound semiconductor radiation detectors, CRC Press, Boca Raton,  
613 2012.

614

615 <sup>12</sup>A. Owens, S. Andersson, R. Den Hartog, F. Quarati, A. Webb, E. Welter, Nucl. Instr.  
616 and Meth. A 581 (2007) 709.

617

618 <sup>13</sup>A. Owens, M. Bavdaz, V. Gostilo, D. Gryaznov, A. Loupilov, A. Peacock, H. Sipila,  
619 Nucl. Instr. and Meth. A 487 (2002) 435.

620

621 <sup>14</sup>A. Owens, A. Peacock, M. Bavdaz, G. Brammertz, F. Dubecky, V. Gostilo, D.  
622 Gryaznov, N. Haack, M. Krumrey, A. Loupilov, Nucl. Instr. and Meth. A 491 (2002)  
623 444.

624  
625 <sup>15</sup> J. H. Hubbell, *Int. J. Appl. Radiat. Is.* 33 (1982) 1269.  
626  
627 <sup>16</sup>R. Jenkins, R. W. Gould, D. Gedcke, *Quantitative X-ray Spectrometry, Second Ed.*,  
628 CRC Press, New York, 1995.  
629  
630 <sup>17</sup>S. Minagawa, M. Kondow, *Electron. Lett.* 25 (1989) 758.  
631  
632 <sup>18</sup>Keithley Instruments, Inc, *Model 6487 Picoammeter/Voltage Source Manual*, 6487-  
633 901-01 Rev B, Cleveland, 2011.  
634  
635 <sup>19</sup>Hewlett Packard, *Model HP4275A Multi-Frequency LCR Meter Manual*, 04275-  
636 90004, Tokyo, 1990.  
637  
638 <sup>20</sup>G. Bertuccio, P. Rehak, D. Xi, *Nucl. Instrum. Meth. Phys. Res. B* 326 (1993) 71.  
639  
640 <sup>21</sup>U. Shotzig, *Applied Radiation and Isotopes* 53 (2000) 469.  
641  
642 <sup>22</sup>G. Lioliou, A. M. Barnett, *Nucl. Instrum. Meth. Phys. Res. A* 801 (2015) 63.  
643  
644 <sup>23</sup>G. A. Bertuccio, A. Pullia, G. De Geronimo, *Nucl. Instrum. Meth. Phys. Res. A* 380  
645 (1996) 301.  
646  
647 <sup>24</sup>E. Gatti, P. F. Manfredi, M. Sampietro, V. Speziali, *Nucl. Instrum. Meth. Phys. Res.*,  
648 *A* 297 (1990) 467.

649 <sup>25</sup>Vishay Siliconix, *2N4416/2N4416A/SST4416 N-Channel JFETs Data Sheet*, 70242  
650 S-50147 Rev. H, Selb, 2005.

651 <sup>26</sup>G. Bertuccio, D. Macera, C. Graziani, M. Ahangarianaghari, *IEEE Nuclear Science*  
652 *Symposium and Medical Imaging Conference (NSS/MIC)* (Seattle, WA, 8-15  
653 November 2014)

654 <sup>27</sup>G. W. Fraser, *X-ray Detectors in Astronomy*, Cambridge University Press,  
655 Cambridge, 1989.

656 <sup>28</sup>G. Bertuccio, D. Maiocchi, *J. Appl. Phys.* 92 (2002) 1248.

657 <sup>29</sup>G. Bertuccio, R. Casiraghi, *IEEE Trans. Nucl. Sci.* 50 (2003) 175.

658 <sup>30</sup>A. M. Barnett, J. E. Lees, D. J. Bassford, J. S. Ng, *J. Inst.* 7 (2012) P06016.  
659

660 <sup>31</sup>M. D. C. Whitaker, S. Butera, G. Lioliou, A.M. Barnett, *J. Appl.Phys.* 122 (2017)  
661 034501.

662 <sup>32</sup>K. Lamkaouchi, A. Balana, G. Delbos, W. J. Ellison, *Meas. Sci. Technol.* 14 (2003)  
663 444.

664 <sup>33</sup>A. M. Barnett, J. E. Lees, D. J. Bassford, *Appl. Phys. Lett.* 102 (2013) 181119.

- 665 <sup>34</sup>G. W. Fraser, A. F. Abbey, A. Holland, K. McCarthy, A. Owens, A. Wells, Nucl.  
666 Instrum. Meth. Phys. Res., A 350 (1994) 368.
- 667 <sup>35</sup>M. N. Mazziotta, Nucl. Instrum. Meth. Phys. Res., A 584 (2008) 436.
- 668 <sup>36</sup>C. A. Klein, J. Appl. Phys. 39 (1968) 2029.
- 669 <sup>37</sup>G. Bertuccio, A. Pullia, J. Lauter, A. Forster, H. Luth, IEEE Trans. Nucl. Sci. 44  
670 (1997) 1.
- 671 <sup>38</sup>A. Owens, M. Bavdaz, H. Andersson, T. Gagliardi, M. Krumrey, S. Nenonen, A.  
672 Peacock, I. Taylor, L. Tröger. Nucl. Instrum. Meth. Phys. Res., A. 484 (2002) 242.
- 673 <sup>39</sup>S. Butera, G. Lioliou, A. B. Krysa, A. M. Barnett. Nucl. Instrum. Meth. Phys. Res.,  
674 A. 879 (2017) 64.